Comparison of Implicit Time-stepping to the Scheme with "Apparent Heat Capacity" for a Thermal Model of Permafrost with Surface Terrain Dependent Boundary Conditions

Malgorzata Peszynska[0000−0001−5013−7943] and
Praveeni Mathangadeera[0009−0006−1664−2288]

Abstract In this paper we consider a nonlinear heat equation describing thawing and freezing of permafrost soils with the time varying surface boundary condition. We compare two schemes for time discretization: a conservative fully implicit one and a non-conservative sequential approach which uses the so called apparent heat capacity. We show that the differences between the schemes can be significant if the time step is large and when the inputs to the problem change abruptly. We also show that a simple variant of sequential scheme with arithmetic average and an extra iteration does not give consistency but gives better agreement with the implicit approach.

1 Introduction

In this paper we discuss two time-stepping schemes denoted by (IMP) and (SEQ) for a model of thawing/freezing of soils in permafrost regions (e.g., in the Arctic); we follow the physical models and scenarios known from geophysical literature [4, 17, 12]. In particular, we are interested in realistic scenarios when the soils respond to the daily, seasonal, and long-term variation of the temperature at the ground surface, and these variations depend on the atmospheric temperature and other physical parameters [2]. We use our earlier work on conservative spatial discretization combined with implicit time stepping (IMP) described in [1, 10, 16]. In this paper we also consider a different non-conservative time stepping scheme (SEQ) which is easy to implement and is quite popular in the geophysical literature. We compare these two algorithms (IMP) and (SEQ) and discuss their pros and cons for the scenarios involving highly variable boundary conditions.

Malgorzata Peszynska
Oregon State University, Corvallis, OR 97331, USA e-mail: mpesz@math.oregonstate.edu

Praveenin Mathangadeera
Oregon State University, Corvallis, OR 97331, USA e-mail: mathangp@oregonstate.edu

Specifically, we consider a doubly nonlinear heat equation posed in a soil region $\Omega \subset \mathbb{R}^d$ solved for the enthalpy w, temperature u, and liquid fraction χ

$$\partial_t(w) - \nabla \cdot (k(u)\nabla u) = 0,\ x \in \Omega, t > 0. \tag{1a}$$

$$w = \alpha(u) = C(u) + L\eta\chi(u), \tag{1b}$$

where the constitutive empirical relationships for the heat enthalpy $\alpha(u)$, its capacity portion $C(u)$, liquid fraction $\chi(u)$, and heat conductivity $k(u)$, respectively, will be given below. Also, L, η are positive parameters denoting the latent heat and porosity. The model is completed with the time-dependent Dirichlet boundary conditions on the Dirichlet portion Γ_D of the boundary $\partial\Omega$, and with Neumann conditions on its complement, and initial conditions

$$u|_{\Gamma_D} = u_D;\ k\nabla u \cdot \nu|_{\partial\Omega\setminus\Gamma_D} = g_N; t > 0, \tag{1c}$$

$$u(x,0) = u_{init}(x), x \in \Omega. \tag{1d}$$

The primary difficulty is the double nonlinearity of the model and the lack of smoothness of $C(u), \chi(u)$ and $k(u)$ at $u = 0$. (Other difficulties arise when the soil is heterogeneous [16]). In general, $C(\cdot)$ is continuous monotone strictly increasing and Lipschitz on $\mathbb{R}$ and differentiable except at $u = 0$. Also, $\chi(u)$ is a continuous monotone nondecreasing Lipschitz function with values in $[0, 1]$ and is smooth except at $u = 0$ with a large gradient as $u \to 0^-$. These properties make $\alpha(u)$ a monotone increasing piecewise smooth function, with an inverse α^{-1} featuring similar properties. In turn, $k(u)$ is bounded, uniformly positive and continuous.

In consequence, the model (1) has to be understood in terms of distributions, and its weak solutions to (1) feature a free boundary $S = \{(x,t) : u(x,t) = 0\}$. Generally, the solutions to (1) are smoother than those to Stefan problem [14] where χ may be discontinuous or multivalued at $u = 0$; see the simulations in the supplement to [10].

Remark 1 In some applications focused literature [4] $\chi(\cdot)$ is considered discontinuous or multi-valued similarly to Stefan problem, and $\alpha(\cdot)$ and $k(\cdot)$ follow suit. The (IMP) scheme works well with these as we show in [1], but the consideration of (SEQ) raises questions; a discussion of these is left for future work.

The numerical schemes for (1) present challenges well documented in our work [1, 10, 16] on conservative discretizations involving spatial discretization with lowest order mixed finite elements on rectangular grid implemented as CCFD (cell-centered finite differences), combined with fully implicit approaches using w or u as the primary unknowns. The mentioned conservation properties are essential in heterogeneous soils [16] as well as when the thermal model is extended to be a part of coupled thermal-flow (TpH) model presented in [8] or thermal-flow-mechanical model (TpHM) in [17, 15].

However, the fully implicit approach is complicated, because an explicit closed form of $\alpha(u)$ and of $\alpha^{-1}(u)$ may not be available or might be computationally expensive to evaluate. These difficulties are likely the reason why the schemes reported in most of the applications literature including [12, 2] apply the chain rule

to write $\partial_t w = c_{app}(u)\partial_t u$, with the "apparent heat capacity" $c_{app}(u)$ so that

$$c_{app}(u) = \frac{d\alpha}{du} = \frac{dC}{du} + L\eta\frac{d\chi}{du}, u \neq 0; \quad \alpha(u) = \int_0^u c_{app}(v)dv. \tag{2}$$

The issue is that c_{app} is discontinuous at $u = 0$; it also features a sharp gradient as $u \to 0^-$; see Figure 1. The associated numerical difficulties have not been well studied in the applications literature with a notable exception of [4] who write $\partial_t w = \frac{dC}{du}\partial_t u + L\eta\partial_t\chi$ and treat $\partial_t\chi$ implicitly. However, perhaps partly due to their non-conservative choice of spatial discretization (nodal finite elements), the results in [4] still feature some oscillations seemingly related to the mass lumping combined with the use of $\frac{dC}{du}$ and the associated lack of maximum principle. In turn, the presentation of the numerical schemes in other applications papers is either absent or is somewhat obscured by the use of field-specific vocabulary and notation specific to each paper and their objectives, and is missing details on the discretization; only [4] presents results corresponding to more than one scheme.

It is the purpose of this paper to compare the implicit (IMP) and the sequential scheme (SEQ) with c_{app} on simple examples for which we demonstrate the similarity and differences and advantages and disadvantages, while we keep the spatial discretization conservative.

Outline. In Section 2 we provide details of the model (1) and its numerical discretization. In Section 3 we compare the implicit and sequential schemes. In Section 4 we conclude and present future and current work.

2 Details of Model (1) and Numerical Discretization

We now make precise the data $\alpha(\cdot), k(\cdot)$ in (1), which completes the presentation of the model. We also define the numerical schemes. In Section 2.4 we also define an algorithm to determine the surface boundary conditions depending on the terrain.

2.1 Constitutive Data

We define $\chi(\cdot)$ first. We adopt the choice from [17], and refer to [11] for a comprehensive list of other $\chi(\cdot)$ called SFC. Given some $b > 0$, we set

$$\chi(u) = 1, u \geq 0, \text{ and } \chi(u) = e^{bu}, u < 0. \tag{3}$$

Next we use thermal soil data from [4, 2, 1, 10, 16] and use volumetric SI units; see [8] for a detailed comparison and a discussion of assumptions and physical units.

We assume the soil porosity $\eta = 0.32$ is fixed and let $L \approx 3.3 \times 10^8$ so $\eta L \approx 10^8$. The volume fractions of rock and water components are denoted by $\nu_r = 1 - \eta$ and $\eta = \eta(1 - \chi_l + \chi_l) = \nu_i + \nu_l$ where $\nu_i = \eta(1 - \chi_l)$ is the frozen volume fraction,

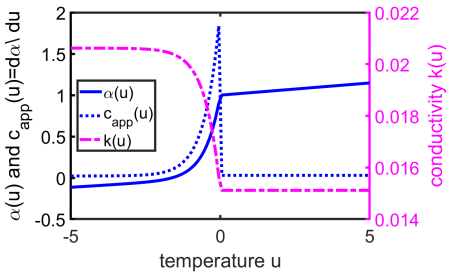

Fig. 1 Plot of $\alpha(u)$, $c_{app}(u) = \frac{d\alpha}{du}$ (left axis, scaled by 10^2) and $k(u)$ (right axis, scaled by 10^{-2}) from Section 2.1.

and $\nu_u = \eta\chi_l$ is the unfrozen volume fraction. We apply arithmetic weighting to the heat capacities building from the thermal properties of rock, ice, and water [2, 4, 10] with $C(u) = \int_0^u c(v)dv$, where $c_f = \eta c_i + (1-\eta)c_r$, $c_u = \eta c_l + (1-\eta)c_r$ and

$$c(u) = c_f + \chi(u)(c_u - c_f); \quad c_l = 4.19 \times 10^6, c_i = 1.94 \times 10^6, c_r = 2.36 \times 10^6,$$

The heat conductivities are weighted similarly

$$k(u) = k_r\nu_r + k_l\nu_l(u) + k_i\nu_i(u); \quad k_l = 0.58, k_i = 2.30, k_r = 1.95.$$

Next we multiply (1) by $\frac{10^6}{L\eta}$, rescale $\tilde{c}_p = \frac{c_p}{\eta L}$, and set the time unit 1 to correspond to 10^6[sec] $\approx$ 11.57 [day] which fits the characteristic time of freezing/thawing. (We keep the same notation t). We also set $\tilde{k}_p = 10^6 \frac{k_p}{\eta L}$ for every $p = r, i, l$. We have now $\tilde{c}_f = 2.21 \times 10^{-2}$; $\tilde{c}_u = 2.94 \times 10^{-2}$, $\tilde{k}_f = 2.06 \times 10^{-2}$, $\tilde{k}_u = 1.51 \times 10^{-2}$,

$$\frac{\alpha(u)}{\eta L} = (\tilde{c}_u - \tilde{c}_f)\int_o^u \chi(v)dv + \tilde{c}_f u + \chi(u); \quad \frac{k(u)10^6}{L\eta} = \tilde{k}_f + (\tilde{k}_u - \tilde{k}_f)\chi(u). \quad (4)$$

We illustrate in Figure 1: $\chi(u), k(u), \alpha(u)$ are continuous, but $\alpha(u)$ is not differentiable at $u = 0$, and features a large gradient as $u \to 0^-$ with a discontinuous $c_{app}(u)$. In turn, $k(u)$ is nonnegative and bounded.

2.2 Fully Implicit Conservative Scheme (IMP) for (1)

We consider a rectangular grid covering Ω, with midpoints $(x_j)_{j=1}^J$, with uniform spacing with parameter h for simplicity. We note the region need not be rectangular, and the numbering $j = 1, \ldots J$ need not be of consecutive cells. We also use fully implicit backward Euler scheme at $t^1, t^2 \ldots t^n, \ldots$, with time step τ considered uniform for simplicity of presentation, $t^0 = 0$ and $t^{n+1} = t^n + \tau$. We approximate the solutions $u(x_j, t^n) \approx U_j^n$, and similarly $W_j^n \approx w(x_j, t^n)$, $\Upsilon_j^n \approx \chi(x_j, t^n)$. These are collected in $U^n = (U_j^n)_j$, $W^n = (W_j^n)_j$, $\Upsilon^n = (\Upsilon_j^n)_j$.

The fully implicit formulation reads: at every time step t^n, solve

$$\begin{aligned} \tfrac{1}{\tau}(W^n - W^{n-1}) + A(U^n)U^n = G^n; \\ W_j^n = \alpha(U_j^n),\ \Upsilon_j^n = \chi(U_j^n),\ j = 1, \dots J. \end{aligned} \tag{5}$$

Here $A(U)$ is a symmetric positive definite matrix and $A(U)U$ approximates $-\nabla \cdot k(u)\nabla u$ with the boundary condition (1c) included in the term G^n; see [1, 16] for details. We also note that the mass matrix in (5) is the rescaled identity matrix which is formally absorbed under A. For $n = 0$ we discretize (1d).

The system (1) is nonlinear semi-smooth and must be solved by iteration, e.g., by semi-smooth Newton using either W or U as a primary unknown. We refer to [16] for a discussion of advantages and disadvantages, and to [9] for analysis of a more general model involving non-equilibria and hysteresis. In particular, resolving $W_j^n = \alpha(U_j^n)$ or $U_j^n = \alpha^{-1}(W_j^n)$ requires an explicit formula for $\alpha(u)$ or its inverse, or a local nonlinear solver. This may be computationally expensive.

Remark 2 Obtaining closed form algebraic formulas for $\alpha^{-1}(w)$ and even for $\alpha(u)$ may be unfeasible, e.g., if $\chi(u)$ is given by e^{-bu^2} [3], or if there are further nonlinearities, e.g., when $c_l = c_l(u)$ [7, 2]. Further difficulties arise when the soil is not fully saturated and when the model accounts for the presence of air.

These difficulties motivate an alternative approach to (IMP) based on (2).

2.3 Sequential Formulation (SEQ) with c_{app} in (2)

To use (2), we define the diagonal matrix $C_{app}(U)$ with $C_{app,jj}(U) = c_{app}(U_j)$ and replace (5) with a nonlinear problem solved by iteration $m = 1, \dots M$

$$\tfrac{1}{\tau} C_{app}(U^*)(U^{n,m} - U^{n-1}) + A(U^{n,m-1})U^{n,m} = G^n. \tag{6}$$

To choose U^*, we can set $U^* = U^{n-1}$ so that (6) is linear. Alternatively we can use $U^* = U^{n,m-1}$ and iterate $m = 1, 2, \dots M$, with $U^{n,0} = U^{n-1}$. The choice of arithmetic average $U^* = \frac{U^{n,m-1}+U^{n-1}}{2}$ with $M = 2$ works well as a predictor-corrector.

Remark 3 Integrating $\int_{t^{n-1}}^{t^n} \partial_t w(\cdot, s)ds \approx W^n - W^{n-1}$ explains why (5) is conservative, but also reveals that (6) is inconsistent and not conservative. This follows because there is no U^* so that $W^n - W^{n-1}$ equals $c_{app}(U^*)(U^n - U^{n-1})$, and no specific choice of U^* can make the solutions to (6) consistent with (5).

2.4 Surface Boundary Condition

In our simulations we need to define $u_D(x,t), x \in \Gamma_D, t > 0$ in (1c). Specifically, we require the knowledge of the surface temperature $u_S(x,t) = u_D(x,t)|_{\Gamma_s}$ where $\Gamma_s \subset \partial\Omega$ represents the surface of the soil.

To this aim we follow closely [2] who postulate that at every point x,t, $T_{so}(x,t)$ [°K] $= u_S(x,t)$ [°C] + 273.15 depends on the atmospheric temperature $T_a(x,t)$ [°K] and on a variety of physical conditions including the air pressure and the temperature dew point, the surface albedo $\alpha(x,t)$, and other parameters $X_1, X_2, \ldots X_9$ which we derive from the formulas in [2], and other physical data in [5, 6]. Given a fixed α, T_a, we find the surface temperature T_{so} as the root to

$$f(\alpha, T_a, T_{so}) = (1-\alpha)X_1 + X_2(1 - e^{-X_3^{\frac{T_a}{2016}}}){T_a}^4 + X_4{T_{so}}^4 + \frac{1}{1+X_5\frac{(T_a - T_{so})}{T_a}}[X_6(T_a - T_{so}) + X_7] + X_8(T_{so} - X_9) = 0, \quad (7)$$

where $X_1 = 1361, X_2 = 6.12\times10^{-8}, X_3 = 3.72, X_4 = -5.10\times10^{-8}, X_5 = 39.24, X_6 = 48.97, X_7 = 16095.745, X_8 = -1.02, X_9 = 272$.

The function $f(\alpha, T_a, T_{so})$ is quite complicated and on a first glance it is not clear whether it is even well defined, and if it has a root. Figure 2 shows its plot for three choices of albedo parameter α corresponding to the snow covered land, vegetation covered land, and water covered land, respectively. Next we collect atmospheric data for $T_a(x,t)$ from [13]; for this paper we choose the data for October 2023 in Gulkana, Alaska. Then, for each $T_a(x,t), \alpha(x,t)$ we find the corresponding $T_{so}(x,t)$ as the root of (7). In practice, we find $T_{so}(x,t)$ by interpolating a look-up table calculated off-line for a collection of $\{T_a, \alpha\}$.

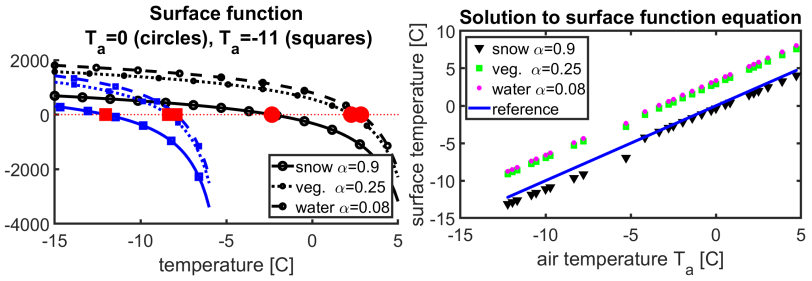

Fig. 2 Illustration of Section 2.4, with all temperature given in [°C]. Left: plot of $f(\alpha, T_a, T_{so})$ given by (7) for $T_a = 0$ (circles) and $T_a = -11$ (squares) and three choices of albedo, over a range of T_{so}, with the roots for each α and T_a marked with red circles and squares. Right: a scatter plot of T_{so} corresponding to the three choices of albedo for a range of input air temperature T_a values found from [13]. It appears that T_{so} for snow is close to T_a, but that for water and vegetation is about 4 [°C] larger than T_a.

3 Simulation Results

Now we illustrate the difference between U^{IMP} and U^{SEQ} when these respond to the varying surface boundary conditions.

3.1 Computational Results for 1D

Our first example in d=1 shows that the U^{SEQ}, Υ^{SEQ} are close to U^{IMP}, Υ^{IMP} even if the boundary condition is rough; the closeness improves as the time step $\tau \downarrow$. We use Newton's method for the IMP scheme (5) with absolute tolerance 10^{-8}, and the simple iteration with $M = 2$ and $U^* = \frac{U^n + U^{n-1}}{2}$ in the SEQ scheme (6).

Let $\Omega = (0, 1)$, $J = 50$, and $T = 3$ (about 33 [days]), and consider

$$\text{(ROUGH)}\quad u_{init}(x) = -5, u(0,t) = 4 \quad u(1,t) = -5. \tag{8a}$$

$$\text{(SMOOTH)}\ u_{init}(x) = -5, u(0,t) = \begin{cases} -5 + 4t, & t \le 1; \\ 4, & 1 < t; \end{cases} \quad u(1,t) = -5, \tag{8b}$$

where $u_D(t)$ in (8a) and (8b) feature a discontinuity at $t = 0$ and $t = 1$, respectively. We simulate the problem with (IMP) and (SEQ) schemes and plot the solutions in Figure 3. We also study $\Delta U|_t = ||U^{IMP}(\cdot, t) - U^{SEQ}(\cdot, t)||_\infty$.

For (8a) we see that the $\Delta U|_t$ is small when τ is small and $M = 2$. Specifically, $\Delta U|_{t=1}$=0.74,0.35,0.06 for $M = 2$, and $\Delta U|_{t=1}$=1.12,0.62,0.33 for $M = 1$, and $\tau = 0., 0.2, 0.1$, respectively. For (8a) we see negligible $\Delta U|_{t=1}$ but a considerable size of $\Delta U|_{t>1, M=1}$ even when $\tau = 0.5$.

3.2 Computational Results for 2D and Surface Boundary Conditions

In our next example we simulate the case when the top boundary $u_S(x, t)$ depends on the topography of the surface. We consider $\Omega = (0, 1)^2$ and use homogeneous Neumann boundary conditions everywhere except at the top of the domain so that $\Gamma_D = \Gamma_S = (0, 1) \times \{1\}$. The grid over Ω is 50×40, and the time step is 1 [day].

We study the (IMP) and (SEQ) schemes when the boundary conditions depend on the location due to the topography of the domain as in Section 2.4. In particular, we assume that $\Gamma_{water} = \Gamma_S \cap \{x : x > 0.5\}$ is in a marshy region covered by water with the albedo $\alpha = 0.08$. The other half $\Gamma_{snow} = \Gamma_S \cap \{x : x < 0.5\}$ is covered by the snow with the albedo equal $\alpha = 0.9$. We also assume that the atmospheric temperature changes over $t \in (0, 31)$ [day] from -12 to 0. Based on Section 2.4 we hypothesize that $u_S(x, t)$ changes from -12 to 0 on Γ_{snow}, and from -8 to 4 for Γ_{water}. We assume also that $u_{init}(x) = -12$.

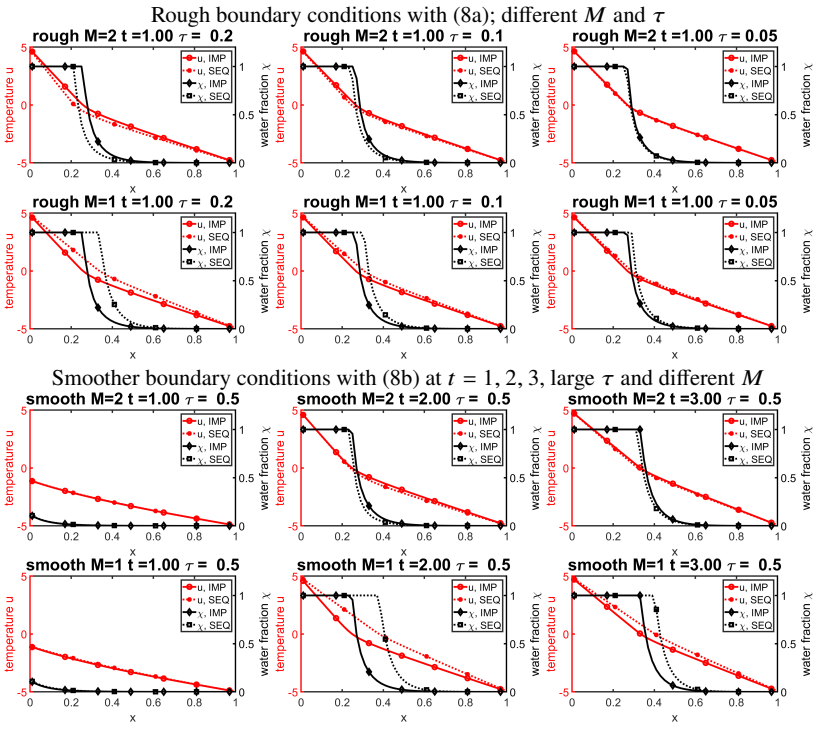

Fig. 3 Results of Section 3.1: in the top two rows we plot $U, \Upsilon|_{t=1}$ for (8a) with $M = 2, 1$. In bottom two rows we use (8b) and plot $U, \Upsilon|_{t=1,2,3}$ for large $\tau = 0.5$.

We apply the (IMP) and (SEQ) schemes and find that both are robust. The solutions are plotted in Figure 4. Newton's scheme for (IMP) converges robustly, and requires at most 4 iterations with relative and absolute tolerance set up as 10^{-6} and 10^{-12}, respectively. The difference between the solutions to (IMP) and (SEQ) is not large as seen from the plots. In fact we find $\Delta U|_{t=31} = 0.23$.

4 Summary

In this paper we compare two time-stepping schemes: an implicit scheme (IMP) and (SEQ) based on chain rule. We find that both schemes are robust, and with small enough time step, the (SEQ) with arithmetic average produces results close to those for (IMP). The difference between (IMP) and (SEQ) can be significant if the boundary conditions change abruptly, such as when using realistic surface boundary conditions.

More work is needed, in particular, to study the sensitivity of the solutions to the surface boundary equation, and to consider (SEQ) when χ is discontinuous.

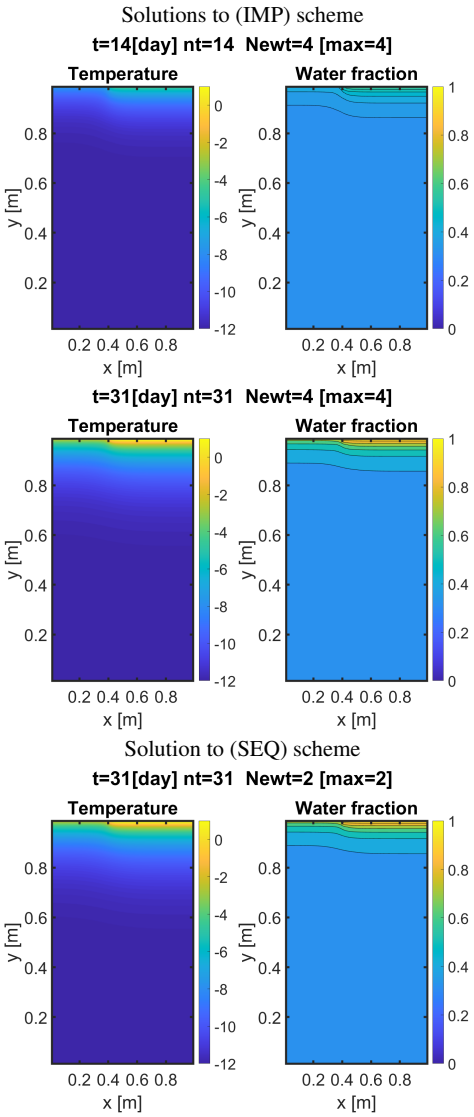

Fig. 4 Illustration of simulation from Section 3.2 with the (IMP) and (SEQ) schemes with surface boundary conditions. We show contour plots of U, Υ (left and right, respectively) at time $t = 14$ and $t = 31$ days. The temperature is higher and water fraction is larger in the right portion of Ω due to the top boundary condition on Γ_{water} higher than on Γ_{snow}.

Acknowledgements We thank the organizers of ENUMATH 2023 and the editors of this special volume of proceedings, as well as the anonymous referees. We also thank Lisa Bigler and Naren Vohra for useful discussions on research in [1, 10, 16] related to this paper. This research was partially supported by the grants NSF DMS-1912938 "Modeling with constraints and phase transitions in porous media", and NSF DMS-2309682 "Computational mathematics of Arctic processes".

References

1. Lisa Bigler, Malgorzata Peszynska, and Naren Vohra. Heterogeneous Stefan problem and permafrost models with P0-P0 finite elements and fully implicit monolithic solver. *Electronic Research Archive*, 30(4):1477–1531, 2022.
2. Feng Ling and Tingjun Zhang. A numerical model for surface energy balance and thermal regime of the active layer and permafrost containing unfrozen water. *Cold Regions Science and Technology*, 38(1):1–15, 2004.
3. Jeffrey M. McKenzie, Clifford I. Voss, and Donald I. Siegel. Groundwater flow with energy transport and water–ice phase change: Numerical simulations, benchmarks, and application to freezing in peat bogs. *Advances in Water Resources*, 30(4):966–983, 2007.
4. Dmitry Nicolsky, Vladimir Romanovsky, and Gennadiy Tipenko. Using in-situ temperature measurements to estimate saturated soil thermal properties by solving a sequence of optimization problems. *The Cryosphere*, 1, 11 2007.
5. Anne DW Nuijten and Knut V Høyland. Modelling the thermal conductivity of a melting snow layer on a heated pavement. *Cold Regions Science and Technology*, 140:20–29, 2017.
6. Rain or Shine. Soil thermal properties. https://open.library.okstate.edu/rainorshine/chapter/13-2-soil-thermal-properties/, 2019. [Online; accessed 30-December-2023].
7. Thomas E. Osterkamp. Freezing and thawing of soils and permafrost containing unfrozen water or brine. *Water resources research*, 23(12):2279–2285, 1987.
8. Malgorzata Peszynska, Zachary Hilliard, and Naren Vohra. Coupled flow and energy models with phase change in permafrost from pore- to Darcy scale: modeling and approximation. *Journal of Computational and Applied Mathematics*, 450:115964, November 2024.
9. Malgorzata Peszynska and Nicholas Slugg. Unified analysis of algorithms for equilibrium, non-equilibrium, and hysteresis models of phase transition in permafrost. In *Advances in the Mathematical Sciences; AWM Series*. Springer, 2024. 26 pages, to appear.
10. Malgorzata Peszynska, Naren Vohra, and Lisa Bigler. Upscaling an Extended Heterogeneous Stefan Problem from the Pore-Scale to the Darcy Scale in Permafrost. *Multiscale Modeling & Simulation*, 22(1):436–475, 2024.
11. Junping Ren, Sai Vanapalli, and Zhong Han. Soil freezing process and different expressions for the soil-freezing characteristic curve. *Sciences in Cold and Arid Regions*, 9:221–228, 07 2017.
12. Joris C. Stuurop, Sjoerd E. A. T. M van der Zee, Clifford I. Voss, and Helen K. French. Simulating water and heat transport with freezing and cryosuction in unsaturated soil: Comparing an empirical, semi-empirical and physically-based approach. *Advances in Water Resources*, 149:103846, 2021.
13. United States. National Weather Service. United States. https://www.weather.gov/, 1999.
14. Augusto Visintin. *Models of phase transitions*, volume 28 of *Progress in Nonlinear Differential Equations and their Applications*. Birkhäuser Boston, Inc., Boston, MA, 1996.
15. Naren Vohra and Malgorzata Peszynska. Iteratively Coupled Mixed Finite Element Solver for Thermo-hydro-mechanical Modeling of Permafrost Thaw. *Results in Applied Mathematics*, 22:100439, 2024.
16. Naren Vohra and Malgorzata Peszynska. Robust conservative scheme and nonlinear solver for phase transitions in heterogeneous permafrost. *Journal of Computational and Applied Mathematics*, 442:115719, 2024.
17. Yao Zhang and Radoslaw Michalowski. Thermal-hydro-mechanical analysis of frost heave and thaw settlement. *Journal of Geotechnical and Geoenvironmental Engineering*, 2015.